Susceptible Frequency Range Definition for Robust Immunity Tests

Ivan Struzhko
University of Twente
Enschede, The Netherlands
ivan.struzhko@utwente.nl

Robert Vogt-Ardatjew
University of Twente
Enschede, The Netherlands
r.a.vogtardatjew@utwente.nl

Frank Leferink
University of Twente
Enschede, The Netherlands
Thales Nederland
Hengelo, The Netherlands
frank.leferink@utwente.nl

***Abstract*— Systems containing lithium-ion batteries are shown to require a longer dwell time to properly perform an immunity test due to their vulnerability to thermal runaway effects. Since thermal processes generally take longer than the standards require for testing, the need for longer dwell time can easily be overlooked. This paper highlights the procedure to estimate the narrow frequency band in which such equipment is the most vulnerable to disturbances, and where longer dwell time should be used. This paper discusses different approaches for determining such a frequency range. In particular, the approach utilizing input impedance measurements is examined in the case of a device containing a lithium-ion battery. The analysis is performed on a simulated circuit as well as based on measurements of an assembled unit representing complex equipment under test.**

Keywords— ***dwell time, immunity testing, simulation, susceptible frequency, thermal phenomena***

I. INTRODUCTION

The need to perform immunity tests (IT) on electrical equipment is a consequence of the rapid development of modern technology. Existing standards provide equipment testing procedures for evaluating immunity to both radiated and conductive disturbances. Although they usually cover basic test parameters such as frequency range, frequency step, dwell time (DT), and stress levels, there are differences in test methods among various standards for different applications (civil, military, etc.). DT is one of the most critical parameters for both conducted and radiated IT. Typically, standards provide minimal DT value, for example, IEC 61000-4-3 [1] and IEC 61000-4-6 [2] define its value for radiated and conducted IT respectively as higher than "the time necessary for the equipment under test (EUT) to be exercised and to respond, but shall in no case be less than 0,5 s." According to RTCA DO-160G [3] DT value for radio frequency susceptibility test "shall be at least one second, exclusive of test equipment settling time", meanwhile in MIL-STD-46IE [4] DT is defined as "the greater of 3 seconds or EUT response time." Thus, DT is dependent on EUT response time, the definition of which is not clear enough. It is reasonable to conclude that the correct DT is that which ensures the occurrence and detection of EUT faults due to EMI. A review of electromagnetic interference (EMI) test reports such as [5], [6] showed that in practice the applied DT value is up to 3 seconds. To find the correct DT, several factors of different origins must be taken into account. Usually, the speed of electromagnetic processes within EUT, the time of its operation cycles, the time required due to test signal modulation, and the settling time of the signal generator are considered in [7]. However, very little attention is paid to the thermal phenomena going on in the EUT. In [8], it was demonstrated that equipment with lithium-ion batteries or other energy storage is prone to failure due to its thermal runaway. The thermal effects can occur over a long period of time, from seconds to minutes or even hours. Therefore, the selection of a suitably long DT is crucial to properly evaluate the EUT immunity.

Frequency step size is also an important parameter for IT. Its value should be sufficiently small to detect the frequencies at which the EUT is most sensitive to disturbances. The structural and coupling resonances within the EUT can result in a response with a high sharpness of the resonance, i.e. large amplitude variation in a very small frequency band. If the step size is too high, the critical frequency can be missed [9].

The obvious solutions to increase the DT and reduce the frequency step size during the IT lead to a significant increase in testing time, making the expensive EMI tests even more expensive. Therefore, [10] proposes approaches for speeding up the test procedure. The methods considered involve increasing the levels of the test signal with a higher frequency step, or using several antennas. However, these solutions result in a sacrifice of accuracy or a necessity to use extra equipment, in addition to partial non-compliance with current standards.

An option, also suggested by the standards [1] and [2], is to perform additional testing in a narrow frequency range with an increased number of frequency steps and greater DT. It seems to be a rather convenient method, as it does not require any additional equipment. It does, however, present the question of determining the relevant frequency ranges at which the EUT is most susceptible to EMI. In [11] a preliminary assessment of the EUT potential susceptible frequencies (SF) is considered as one of the main parts of the risk-based EMC approach implementation. It can provide an increased time- and cost-efficiency, or reliability of the performed IT. The method for determining SF using EUT input impedance is suggested in [11] and [12]. It will be used in this paper for the simulation of the EUT presented in [8] and the analysis of the assembled unit.

This paper aims to emphasize the need to define the SF range, i.e. a range of frequencies where the EUT is particularly susceptible to EMI, for performing the additional IT with sufficient DT value. Thus, the methods to determine the SF proposed in existing research are discussed in Section II. This need is demonstrated by the example of a EUT containing a lithium-ion battery, which is presented in

This project has received funding from the European Union's EU Framework Programme for Research and Innovation Horizon 2020 under Grant Agreement No 955646.

979-8-3503-2400-6/23/$31.00 ©2023 IEEE

detail in Section III. Furthermore, a method for determining the potential SF by performing simple measurements using a vector network analyzer (VNA) is discussed in Section III. Numerical simulation and experimental validation results of that EUT setup are discussed in Section IV and Section V, respectively. And finally, in Section VI, conclusions are presented.

II. Definition of the Susceptible Frequencies

There are many possible solutions for determining the SF, they all have different applications, and are not universal. One factor to consider when specifying the SF is which quantities of the system are linked to EMI effects. For example, in [12], authors perform different conducted and radiated immunity tests using a transverse electromagnetic (TEM) cell, direct power injection (DPI) method, and near-field scanning (NFS) to characterize the susceptibility of commercial op-amp mounted on a printed circuit board (PCB). In this particular case, SF is defined as the frequencies at which the output voltage error is the highest. The frequencies of two out of three identified SF points were very close to the maximum and minimum values of the measured impedance, indicating a potential correlation between these two quantities.

A similar approach is presented in [11], where estimation of the EUT, an electrical scooter, sensitive frequency is proposed to be found from the highest input impedance, measured with a VNA. Afterwards, a differential mode signal was injected using the DPI method into the same points where the input impedance was measured before. The speed of the scooter was chosen as the quantity indicating EMI. Two such occurrences of EMI were registered in the frequency range where the impedance was the highest.

In [8], the SF of the EUT containing a lithium-ion battery was preliminarily determined via a simulation and optimized using measurements. The current in the grounding cable and voltage between the battery terminals were selected as quantities related to EMI in that EUT. This case will be discussed in more detail in the following section.

In [7], the high emission frequencies of the EUT, determined via the radiated emission test, were identified as SFs, following the reciprocity theorem. However, this method does not provide any link to the selection of the quantities indicated EMI of the EUT. The frequencies at which a particular DUT line is most vulnerable to EMI are not necessarily SF for the device as a whole. Therefore, better solutions are necessary to find the SFs with higher accuracy.

III. Case Study

The widespread use of lithium-ion batteries has led to an increasing number of accidents with them. One of the frequently observed possible failure mechanisms is thermal runaway due to high current density [8]. This results in smoke, fire and explosion. The case studied in this paper is based on the system containing a lithium-ion battery presented in [8], shown also here in Fig. 1. This case represents real equipment which is used in transport systems. A load is connected to the positive electrode of the battery and the negative electrode is connected to the reference plate, which represents the chassis of a vehicle. An equivalent electric circuit diagram representing the discussed system is shown in Fig. 2. The equivalent element values of the battery examined in [8] were measured with a network analyzer. The 3.3-meter wire connecting the battery and the load is relatively long and therefore vulnerable to electromagnetic fields. This wire was chosen for performing the bulk current injection (BCI) test of the system.

Preliminarily, this system was simulated to determine the frequency at which the current through the inductance *L3* (grounding wire) and the voltage on the capacitor *C2* (between the first and third electrodes) show the highest values under a 5-mA current injection. The simulation resulted in an SF of 11.3 MHz. Then, the BCI test was performed for this test frequency, and optimized for the highest current in the grounding wire (*L3* on Fig. 2). The peak value of injected current was set at 5 mA - a level much lower than 300 mA, which is the maximum conducted susceptibility test current according to DO-160G [3]. The results showed that even such a low injected current resulted in a 1.5 A current flowing in the grounding wire. It subsequently caused the heating up of the cell metal case to 70°C. It is important to note that this heating took longer than the DT value typically used in such tests and suggested by the corresponding standards. According to the presented temperature measurements, after 3 seconds of testing, the temperature reached 40°C, which is remarkable, but not the cause of the EUT failure. For safety reasons, the test continued until 70°C was reached, which took around 10 seconds. The temperature reached is outside the generally acceptable temperature region for lithium-ion batteries. At this value, the battery structure degrades and a failure may occur [13].

This case demonstrates the need of increasing the DT to values, at which dangerous thermal processes can be detected. This requires solving questions such as which quantity should be monitored and at what frequency must the IT with increased DT be conducted. As the described case shows, the heating of the battery is directly influenced by the current in the wires connecting the battery enclosure to the ground and the voltage between the battery terminals and its enclosure. And they were chosen as such quantities.

The definition of the SF via simulation of the system performance requires high accuracy of the model. Measuring the elements of the equivalent EUT schematic, in particular the lithium-ion battery, is not a trivial task [14] and their values will be different for each individual case. Therefore, a method for assessing SF of the EUT from simple measurements is needed. The possible solution is discussed in the following section.

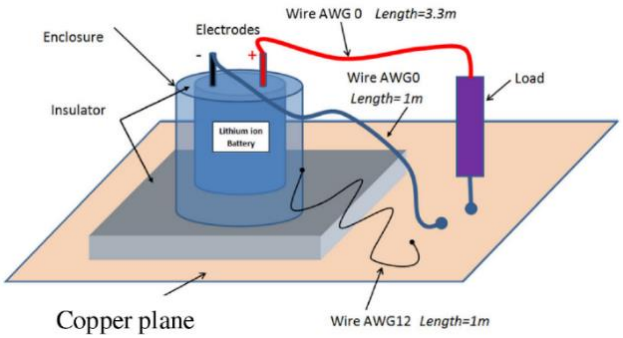

Fig. 1 Battery test setup [8]

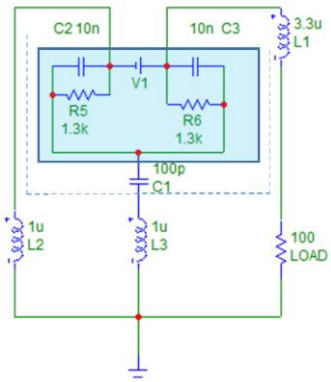

Fig. 2 Equivalent electrical circuit of the battery test setup [8].

IV. Simulation of the Presented EUT Performance

For the EUT described in [8], the authors found a value of SF from simulation and conducting a BCI. To find the link between the input impedance of the system and these results the model of this circuit is designed in LTSpice and shown in Fig. 3. The component values are taken from [8].

The BCI method is modelled as an AC current source *I1* on a wire connected to a positive electrode in series with the load. The simulation is performed in the range from 5 MHz to 30 MHz with 1000 linearly-spaced points. The current in *L3*, which represents the grounding wire, and voltage on capacitor *C2*, which represents the voltage between the negative battery terminal and cell case, are measured and shown in Fig. 4. The results presented in Fig. 4 show that the measured current and voltage reach their peak values at a frequency of about 11.28 MHz, which is similar to the results of the simulation and measurements in [8] – 11.3 MHz. The absolute values of current and voltage at this point are 18.1 A and 12.7 V, respectively.

To represent the VNA measurement proposed in [11], the input impedance measurement between points A-B is performed. As shown in Fig. 5, input impedance reaches a maximum value of 256 kOhm at 11.28 MHz and a minimum value of 250 Ohm at 12 MHz. A frequency close to 11.28 MHz is the resonant frequency for a loop consisting of equivalent elements *L3*, *L4* and *C2*, resulting in significant current circulating through these elements. This simulation shows that in this particular case, a significant current increase in the branch with L3 at 11.28 MHz can be predicted from the VNA measurements.

The next section will present the measurements on the assembled device. To detect its SF, the differential mode voltage will be injected via a waveform generator. To simulate these measurements on the presented model, current source I1 was replaced with a voltage source with an internal resistance of 50 Ohms. In Fig. 6, currents through resistance R_{LOAD} and inductance *L3* are presented. The current I_{LOAD} shows a significant reduction at around 11.28 MHz, which is caused by the large input impedance. However, it is notable that between 9 MHz and 16 MHz, the current through L3 significantly higher than the current I_{LOAD}. At 11.28 MHz the current through *L3* is 3615 times higher than I_{LOAD}. It corresponds to the ratio between injected 5 mA current and current through *L3* during the simulation of the BCI method. This is an indication that, at this frequency, the EUT is most susceptible to failure due to significant current through *L3*.

Therefore, this simulation shows the possibility to detect the SF via such an approach, by determining the ratio of input current and output current, which represents the quantity indicating EMI in this case.

V. Validation of the SF Assessment Method

The results of the simulation in the previous section support the hypothesis that measurements of the EUT input impedance can give an indication of SF. In order to validate this relationship, experiments were carried out on another EUT. The schematic of the assembled unit is based on the presented case with the lithium-ion battery shown in Fig. 2. Unlike the equivalent circuit diagram, the assembled unit contains real components with non-ideal behaviours, including parasitic effects. The voltage source is replaced by a capacitor, as was proposed in [8]. The unit also contains two 1-meter wires and one 3.3-meter wire. The layout of the wires remained unchanged throughout each measurement session. The SMA connector is mounted between a 3.3-meter wire and a resistor representing R_{LOAD} to connect the VNA and waveform generator. Therefore, considering all the uncertainties associated with device component parameters, this unit can be considered as a black box, with input terminals A and B, and a 1-meter wire. It represents the grounding wire from Fig. 2 and the current flowing through it represents EMI.

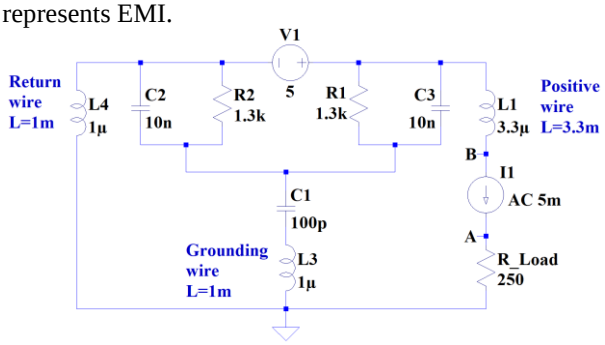

Fig. 3 Model of the battery setup

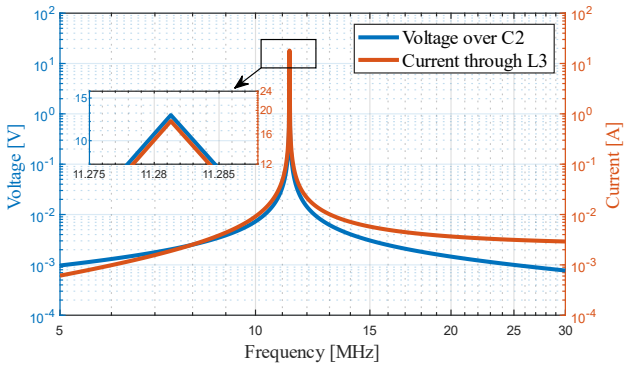

Fig. 4 Output of BCI method simulation

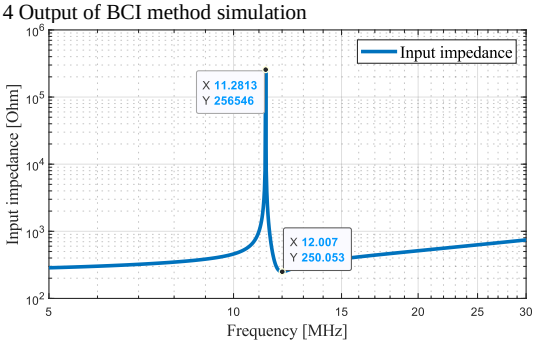

Fig. 5 Input impedance simulation

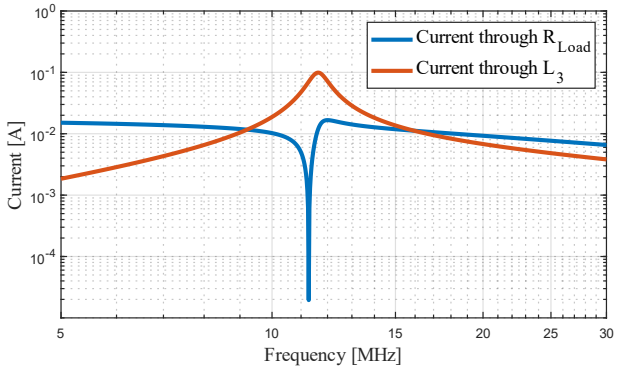

Fig. 6 Currents in R_{LOAD} and *L3* at a constant input voltage level

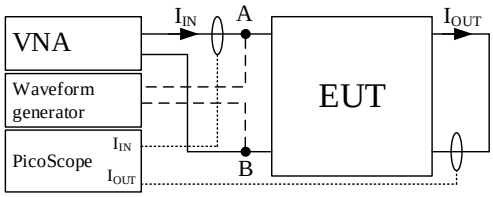

Fig. 7 Measurement setup

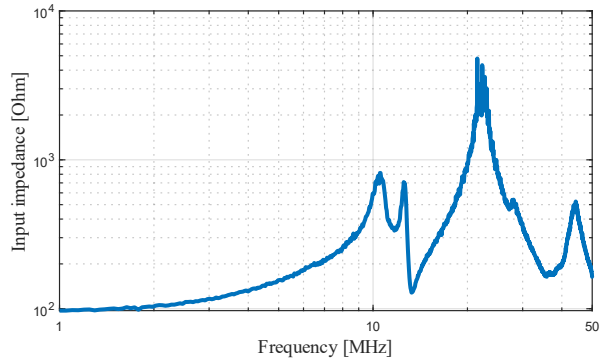

Fig. 8 Input impedance of the assembled unit.

Therefore, considering all the uncertainties associated with device component parameters, this unit can be considered as a black box, with input terminals A and B, and a 1-meter wire. It represents the grounding wire from Fig. 2 and the current flowing through it represents EMI.

The setup for performing the measurements is shown in Fig. 7. The VNA is used for the EUT input impedance measurement presented in Fig. 8. The input impedance reaches the maximum value at the frequency of about 22.9 MHz. In addition, two more peaks can be detected at frequencies 10.3 MHz and 13.9 MHz. Furthermore, the waveform generator is used to inject voltage between points A and B over the frequency range from 1 MHz to 50 MHz with a frequency step of 0.1 MHz. The multichannel oscilloscope with current clamps is used to measure the currents I_{IN} and I_{OUT}. The maximum values of I_{IN} and I_{OUT} at each frequency during the sweeping time are presented in Fig. 9. The input and output currents within the unit during voltage injection are shown in Fig. 9(a) and Fig. 9(b) respectively. In Fig. 9(c) the difference between I_{OUT} and I_{IN} is presented. At a frequency of 14.8 MHz, the output current is significantly higher than the input one. This behaviour indicates that frequencies around 14.8 MHz are susceptible for this device. And in the case of the BCI test, the small current injection at this frequency will result in a significant output current.

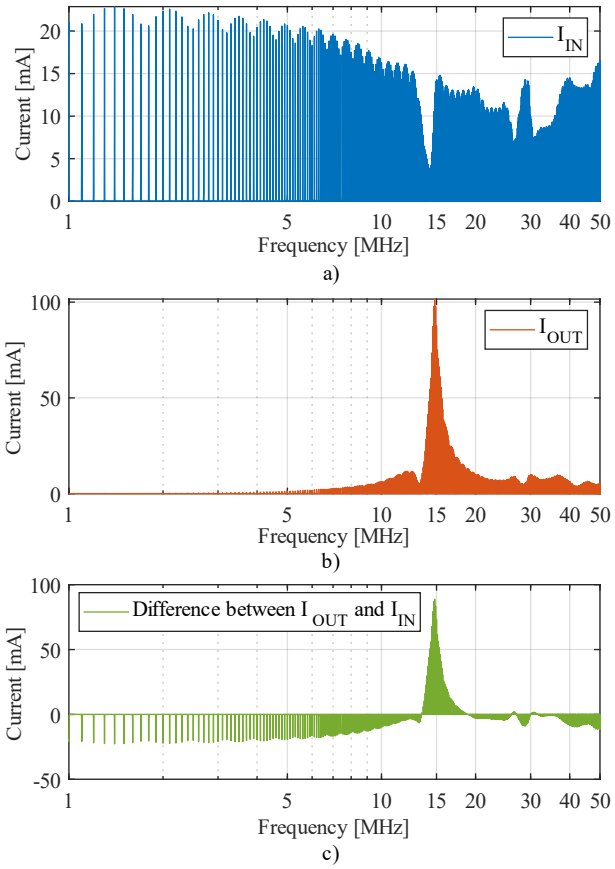

Fig. 9 Input and output current measurements

However, this frequency does not match with frequencies where the input impedance in Fig. 8 shows the maximum. Although this higher current within the circuit is caused by the parallel resonant phenomenon, this resonant contour is not noticeable on the measured input impedance. The custom EUT structure is more complex than discussed in section IV. So another perspective on input impedance analysis is needed to detect SF for such complex devices. The possible approach to addressing this issue will be discussed in the conclusions.

VI. Conclusion

This paper highlights the need for increased DT and smaller frequency steps for immunity testing of equipment containing lithium-ion batteries, as they are extremely sensitive to overheating. Existing IT standards contain a DT value which is not sufficient to detect thermal phenomena in the DUT. Given the potentially serious consequences of overlooking the vulnerability of a device with lithium-ion batteries, additional testing should be included in the testing procedure of such equipment. Raising the DT requires identifying the SF of the EUT to reduce the IT duration. A proposed method, based on measured input impedance analysis, was verified by simulation of the EUT with a lithium-ion battery and examination of the own assembled unit.

One possible solution is to consider the maximum power transfer theorem. At frequencies where the EUT impedance is equal to the complex conjugate of the emission source impedance, the maximum power will be delivered to the EUT. In the case of a VNA or waveform generator, whose impedance is assumed to be purely active, the frequencies

where EUT reactance is close to zero could be considered as SF. Since the EUT here has a purely resistive behaviour, all this energy will be dissipated by the heat loss within the device. An examination of this approach would be one of the next steps for determining the frequencies at which a EUT is most susceptible to EMI.

REFERENCES

[1] IEC 61000-4-3, “Testing and measurement techniques – Radiated, radio-frequency, electromagnetic field immunity test”, 4rd. Ed., Sep. 2020.

[2] IEC 61000-4-6, “Testing and measurement techniques – Immunity to conducted disturbances, induced by radio-frequency fields”, 4th. Ed., Oct. 2013.

[3] RTCA DO-160G, “Environmental Conditions and Test Procedures for Airborne Equipment”, Dec. 2010

[4] MIL-STD-46IG, “Requirements for the control of electromagnetic Interference characteristics of subsystems and equipment”, Dec. 2015.

[5] United Testing Technology, “EMC Test Report. Report No.: UNIA19071704ER-01”, Shenzhen, China, 2019. [Online]. Available: https://www.factorled.com/en/index.php?controller=attachment&id_attachment=647

[6] NTEK Testing Technology, “EMC Test Report. Report No.: NTEK-2013NT0905144E-01”, NTEK, Shenzhen, China, 2013. [Online]. Available: https://tinyurl.com/4bauyxu7

[7] A. N. Vinod, C. Subramanian and S. K. Das, "Optimum dwell time determination for RF immunity test," Proceedings of the International Conference on Electromagnetic Interference and Compatibility '99 (IEEE Cat. No. 99TH 8487), Hyderabad, India, 1997, pp. 57-60, doi: 10.1109/ICEMIC.1997.669760.

[8] E. R. Dubois, H. Kherbouchi and J. Bosson, "Thermal Runaway of Lithium-Ion Batteries Triggered by Electromagnetic Interference," in IEEE Transactions on Electromagnetic Compatibility, vol. 62, no. 5, pp. 2096-2100, Oct. 2020, doi: 10.1109/TEMC.2020.2966743.

[9] K. Armstrong, T. Williams, “EMC testing Part 4 – Radiated immunity“, Cherry Clough Consultants, Stafford, UK, 2007. [Online]. Available: https://www.emcstandards.co.uk/files/d-i_y_emc_testing_2001_part_4_radiated_immunity.pdf

[10] D. Pommerenke, "Methods for speeding up radiated and conducted immunity tests," IEEE International Symposium on Electromagnetic Compatibility. Symposium Record (Cat. No.00CH37016), Washington, DC, USA, 2000, pp. 587-592 vol.2, doi: 10.1109/ISEMC.2000.874686.

[11] V. Gkatsi, R. Vogt-Ardatjew, F. Leferink, “Fast and Curious: Exposure of EMI Vulnerability of an Electric Scooter for a Risk-based EMC Approach”, to be published.

[12] M. Girard, T. Dubois, G. Duchamp and P. Hoffmann, "EMC susceptibility characterization of an operational amplifier-based circuit combining different technique," 2016 International Symposium on Electromagnetic Compatibility - EMC EUROPE, Wroclaw, Poland, 2016, pp. 300-305, doi: 10.1109/EMCEurope.2016.7739244.

[13] S. Ma, M. Jiang, P. Tao, C. Song, “Temperature effect and thermal impact in lithium-ion batteries: A review,” Progress in Natural Science: Materials International, vol. 28, is. 6, 2018, p. 653-666, doi: 10.1016/j.pnsc.2018.11.002.

[14] H. Hackl, D. J. Pommerenke, M. Ibel and B. Auinger, "Extraction of Single Cell Impedance From Battery Module Measurement by Simulation-Based De-Embedding," in IEEE Transactions on Signal and Power Integrity, vol. 1, pp. 112-120, 2022, doi: 10.1109/TSIPI.2022.3199178.

979-8-3503-2400-6/23/$31.00 ©2023 IEEE